Shape-controllable synthesis of indium oxide structures: Nanopyramids and nanorods

Ye Zhang, Hongbo Jia, Dapeng Yu,[a] Xuhui Luo, Zhensheng Zhang, and Xihong Chen
School of Physics, National Key Laboratory of Mesoscopic Physics, and Electron Microscopy Laboratory, Peking University, Beijing 100871, People's Republic of China

Cheoljin Lee
Department of Nanotechnology, Hanyang University, Seoul 133-791, Korea

(Received 10 July 2003; accepted 3 September 2003)

We describe a vapor-phase route to the controllable synthesis of indium oxide micro- and nanopyramids on the silicon wafer via selective epitaxial vapor-solid growth by a methane-assist thermal reduction method. X-ray diffraction, scanning electron microscopy, and transmission electron microscopy revealed that the pyramids were cubic single crystals with a tetragonal symmetry. The size, morphology, and density of pyramids could easily be controlled by tuning reaction parameters. The method has good compatibility with other procedures involved in the microfabrication processes. Laterally grown indium oxide nanorods on the silicon wafer were also prepared via a vapor-liquid-solid mechanism. Those crystalline In_2O_3 nanorods were about 100 nm in diameter and 1 μm in length. The as-synthesized indium oxide nanopyramids and nanorods could offer novel opportunities for both fundamental research and technological applications.

I. INTRODUCTION

The preparation and physical property investigation of indium oxide have drawn much attention due to its remarkable performance on low electrical resistivity (Sn-doped indium oxide), high visible-light transparency (~90%), and high infrared reflectivity.[1,2] In_2O_3 is a versatile wide-band-gap semiconductor (direct band gap: ~3.6 eV)[1] and has widely been used as antireflection (AR)coatings and transparent electrodes in solar cells,[2] transparent electrodes in flat panel displays and organic light-emitting diodes,[2,3] gas sensors,[4] window heaters,[5] varistors,[6] and so forth. Various well-established techniques, such as vacuum evaporation,[7] pulsed laser ablation,[8] magnetron sputtering,[9] electrochemical deposition,[10] sol-gel,[11] and spray pyrolysis[12] have been used to prepare In_2O_3 or Sn-doped indium oxide with different structures (including films, nanobelts, nanowhiskers, and particles).[7–13] However, most of them are amorphous or polycrystalline solids. It is also of interest to grow single-crystalline In_2O_3 or Sn-doped indium oxide with controllable size, structure, and morphologies because of fundamental scientific research interests as well as for practical reasons. Here we report that indium oxide can be made into a tetragonal pyramid-shaped or so-named prism-shaped morphology. The synthesized In_2O_3 pyramids possess a single-crystalline structure with controllable size in mesoscale range and extremely smooth facets. To the best of our knowledge, this is the first time indium oxide with such unusual tip-shaped structure was prepared. Moreover, these peculiar crystallographically well-defined In_2O_3 pyramids can strongly affect intrinsic physical properties of material and offer exciting opportunities for vacuum microelectronic and optoelectronic applications. One of the potential applications of the In_2O_3 pyramids is to be used as cold-cathode field emitters. The small radius of curvature at their tip is expected to lead to an increase of field enhancement factor (β), and hence field emission might be achieved at a low threshold voltage. Furthermore, the density and grain size of In_2O_3 pyramid can easily be modulated to form a film with texture structure suitable for photon trapping.[14] Because In_2O_3 is transparent to ultraviolet and visible light (cut-wavelength: ~344 nm) and conveniently doped with some luminescent centers, it is also possible to utilize the In_2O_3 prisms as efficient optical micro- or nanocavities for laser action.

II. EXPERIMENTAL

A. Nanopyramids

Our experiments were performed in a conventional furnace with a horizontal alumina tube. In a typical process, a film of metal nickel catalyst with 5 nm in thickness

[a]Address all correspondence to this author.
e-mail: yudp@pku.edu.cn

was evaporated onto an n^+-type (100) orientation silicon wafer (resistivity = 0.01 Ω cm) by using the electron beam. The silicon substrate was put downward on an alumina boat loaded with a mixture of granular indium (purity: 99.999%, Shanghai Chemical Reagent Corp., China) and In_2O_3 powder (purity: 99.999%, Shanghai Chemical Reagent Corp.) in a weight ratio of about 10:1. The vertical distance between source and silicon substrate was about 5 mm. Then, the chamber was heated up to 950 °C with a rate of 20 °C/min at a 200 sccm constant flow of argon (99.999%) and atmosphere pressure. Keeping the temperature and argon flow rate, the chamber pressure was pumped to 40 torr. Subsequently, methane (CH_4) was introduced into the furnace chamber under a constant flow rate at 20 sccm for 10 min, and then the furnace was allowed to cool down. A hazily transparent thin deposition layer was found deposited on Si surface.

B. Nanorods

The preparation routine is similar to that of pyramids, but with different reaction parameters as follows: reaction time, 5–7 h; temperature, 1000 °C; gas pressure, atmospheric pressure; gas, only Ar flow, without CH_4 flow; indium source, only metal indium.

C. Characterization

The as-deposited products were characterized by scanning electron microscopy (SEM) [Amray FEG-1910], high-resolution transmission electron microscopy (HR-TEM) [Tecnai F30], nanosized beam energy-dispersive spectroscopy (EDS) [Hitachi-9000NAR, Tokyo, Japan], and x-ray diffraction (XRD) [X'pert MRD-Philips diffractometer, Eindhoven, The Netherlands]. Specimens for HR-TEM and EDS were prepared under a normal ultrasonication process. The field emission was measured in a high-vacuum chamber evacuated to 5×10^{-7} Pa at room temperature. The n^+-type silicon wafer deposited with high density of In_2O_3 pyramids was stuck to a stainless steel support by silver paste to serve as the cathode. The emission current was monitored by a Keithley 485 electrometer.

III. RESULTS AND DISCUSSION

Indium oxide pyramids were prepared on the (100) silicon wafer by the thermal chemical-vapor-deposition method using nickel as the catalyst. The XRD measurement [Fig. 1(a)] and EDS spectrum [Fig. 1(b)] demonstrate that the as-synthesized products are cubic bixbyite In_2O_3 crystals with lattice parameters of $a = 10.1$ Å (consistent with the standard value for cubic In_2O_3) and also show that the phase purity of indium oxide is better than 99%. The morphologies of deposited material were

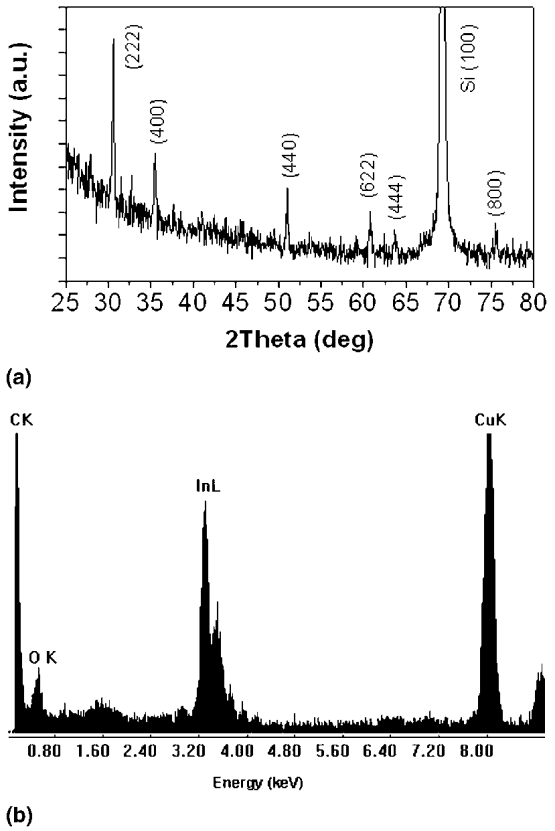

FIG. 1. (a) The XRD diffraction spectrum of indium oxide pyramids on the (100) silicon substrate. (b) EDS spectrum of an indium oxide pyramid.

examined by a scanning electron microscope. As illustrated in Fig. 2(a), a large quantity of pyramids with uniform side length (average value is about 180 nm) are spread over silicon wafer (synthesized at temperature of 950 °C). All of these pyramids are well faceted and possess extremely smooth facets. Only in rare cases, some pyramids were gently truncated. Moreover, these In_2O_3 pyramids exhibited fourfold axial symmetry. Most of these axes show a near vertical alignment to substrate. To further investigate the geometrical characteristics of the In_2O_3 pyramids, we examined a large number of pyramids with SEM from different viewing angles. It is noted that each pyramid is enclosed by four triangle facets and one square bottom-facet that is generally observed parallel to the substrate. high-resolution electron microscopy image and selected-area electron diffraction pattern verified the single-crystalline characteristic of In_2O_3 pyramids [Fig. 2(b)].

Reaction parameters, such as the crystallization temperature, the vapor phase concentration, and the reaction time, can remarkably influence the size, morphology, and density of the products. For example, the higher the growth temperature, the larger the In_2O_3 pyramids with a wider size distribution were formed [Fig. 2(c)]. The density of the pyramids can be controlled by changing the

deposition time. By simply increasing the growth time, a textured In_2O_3 film was developed (Fig. 3). These results demonstrate that we offer a promising route to acquire natively textured indium oxide films, which can act efficiently as both transparent front electrodes and AR coatings in solar cell devices.[14]

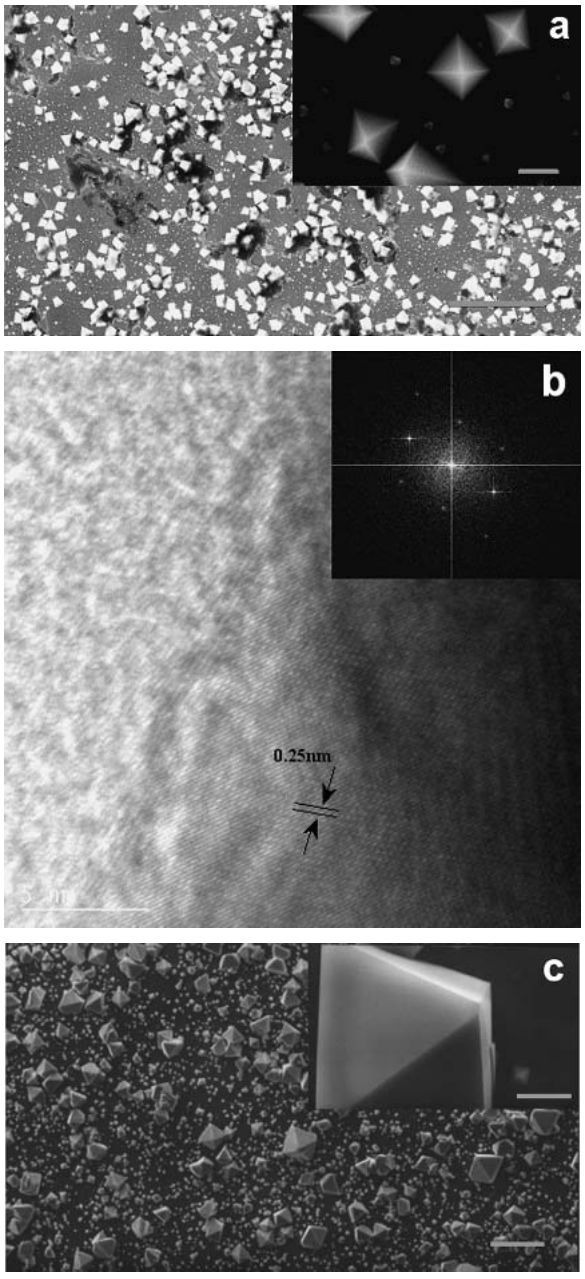

FIG. 2. SEM images of indium oxide pyramids on silicon substrates. (a) Nanopyramids. Mean grain size: approximately 180 nm. Growth condition: CH_4, 20 sccm; Ar, 200 sccm; 10 min; 40 torr; 950 °C. The scale bar corresponds to 5 μm. Inset: The scale bar is 200 nm. (b) The high-resolution transmission electron microscope image of an In_2O_3 pyramid. (c) Micropyramids. Mean grain size: 1–5 μm. Growth condition: CH_4, 20 sccm; Ar, 200 sccm; 10 min; 40 Torr; 1050 °C. The scale bar corresponds to 10 μm. Inset: The scale bar is 1 μm.

The formation of pyramid-shaped morphology is ascribed to preferential adsorption of In/O species on some special crystallographic planes of In_2O_3, the so-called selective epitaxial vapor-solid (VS) growth mechanism. It has been pointed out that the morphology of a cubic crystal phase is generally determined by a ratio (R) between the growth rates along ⟨100⟩ and ⟨111⟩.[15] Octahedra or tetrahedra bounded by energy-stable (111) facets [(111) facets in cubic phase have energy minima because the number of bonds cut by (111) plane is small] will be developed when $R = 1.73$, and cubes bounded by the less stable (100) facets will form if R is reduced to 0.58.[15] As a result, the plane with the slowest growth rate will finally appear as the facets over the other planes. In our case, the epitaxial growth rate of (400) plane is faster than that of (222), therefore, (222) facet tends to appear in the final geometry structure. In this way, indium oxide pyramid abundant in (222) facets will ultimately be formed. Correspondingly, the square bottom facets of pyramid are indexed to (400) plane; meanwhile, triangular ones correspond to (222) planes (Fig. 4). Actually, a

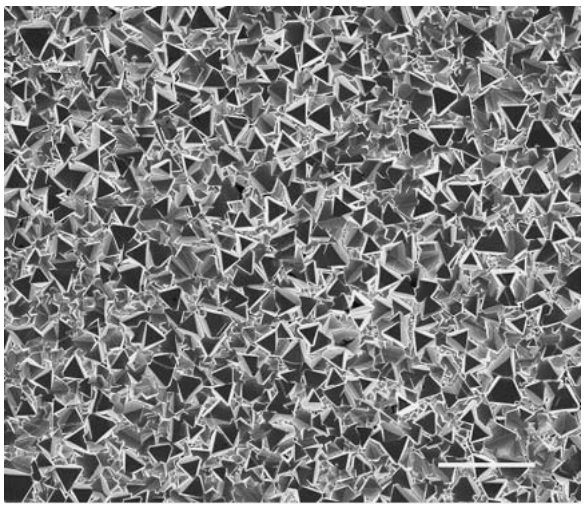

FIG. 3. The SEM image of textured structure acquired by setting reaction time to about 30 min at 1000 °C. The scale bar corresponds to 20 μm.

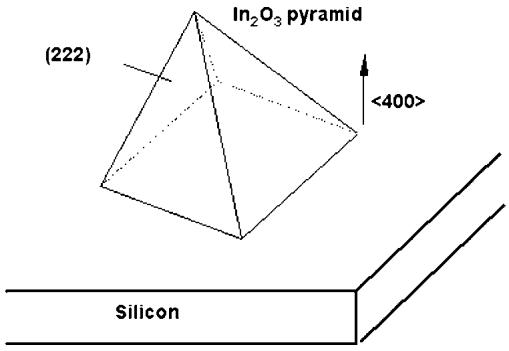

FIG. 4. Schematic view of the pyramid.

similar phenomenon also occurred in formation of silicon pyramids by chemical etching of the (100)-oriented silicon wafer.[16] Chemical etching is known to produce pyramid-shaped pits on the (100)-oriented silicon wafer; those silicon pyramids were produced by exposure of energetically stable (111) planes.[16]

The metal nickel catalyst layer is essential to the formation of In_2O_3 pyramids. SEM observations confirmed that nothing was deposited on the pure silicon wafer in absence of the nickel layer. Upon heating, the nickel film (thickness: 1–5 nm) has been proven to break up into separated nanosized islands.[17] These Ni islands form spontaneously as a means of relieving the strain caused by the mismatch between the Ni lattice and that of the Si substrate. The nickel islands formed on silicon substrate in the heating process at the initial growth stage can provide crystal nucleation sites for growth of pyramids. In other words, Ni islands serves as the "seeds" for pyramid growth.

Obviously, it is impossible for metal indium vapor to feed the growth of In_2O_3 pyramid because of its extremely low vapor pressure (1.8 Pa at 947 °C), especially in our case of a short growth time (typical growth time: 10 min). Volatile oxide species, In_2O, should play a key role as feeding vapor species in supporting the epitaxial growth of pyramids. In_2O was yielded through a methane-assist thermal reduction reaction:

$$In_2O_3\,(s) + CH_4 \rightarrow In_2O\,(g) + CO + H_2O + H_2 \quad . \quad (1)$$

In a word, adsorption of In_2O and O species to Ni nanoparticles initiates crystal growth of In_2O_3. High epitaxial growth rate of (400) plane leads to formation of pyramid morphology of In_2O_3 crystal.

Experimental results showed that no CH_4 resulted in formation of no pyramids (growth time: 10 min). However, we found that In_2O_3 nanorods can be achieved by employing a long growth time (>5 h) in absence of CH_4 flow. SEM images [Fig. 5(a)] reveal that randomly distributed nanorods are laterally deposited on the silicon wafer. The nanorods possess a straight morphology and have predominately around 100 nm in diameter and about 1 μm in length [Fig. 5(a)]. TEM observations also visualize the crystalline characteristic of the nanorods [Fig. 5(b)]. Nearly all of the nanorods terminate at a cubic-faceted or spherical-shaped particle with diameter of about 300 nm [Fig. 5(a), inset]. EDS spectra demonstrate that the nanorods consist of only In and O, and the particles contain Ni, In, and O. This is typical evidence for the vapor-liquid-solid (VLS) dominated growth mechanism.[18] The O element of In_2O_3 crystals may originate from residual oxygen in the chamber. It is a reasonable result because indium vapor seems to be more easily dissolved into Ni droplets compared with In_2O and, hence, in favor of VLS process. In the initiative stage, indium atoms are slowly vaporized and slowly dissolve into Ni nanoparticles to form Ni–In droplets. Continuous dissolution of In and O into In–Ni–O nanodroplet results in supersaturating of In–Ni–O alloy and then one-dimensional growth of In_2O_3. In addition to the straight and homogeneous In_2O_3 nanorods, branched structures have also been observed at times [Fig. 5(c)]. Branched structures can be interpreted by the dislocation model or the secondary nucleation model.[19]

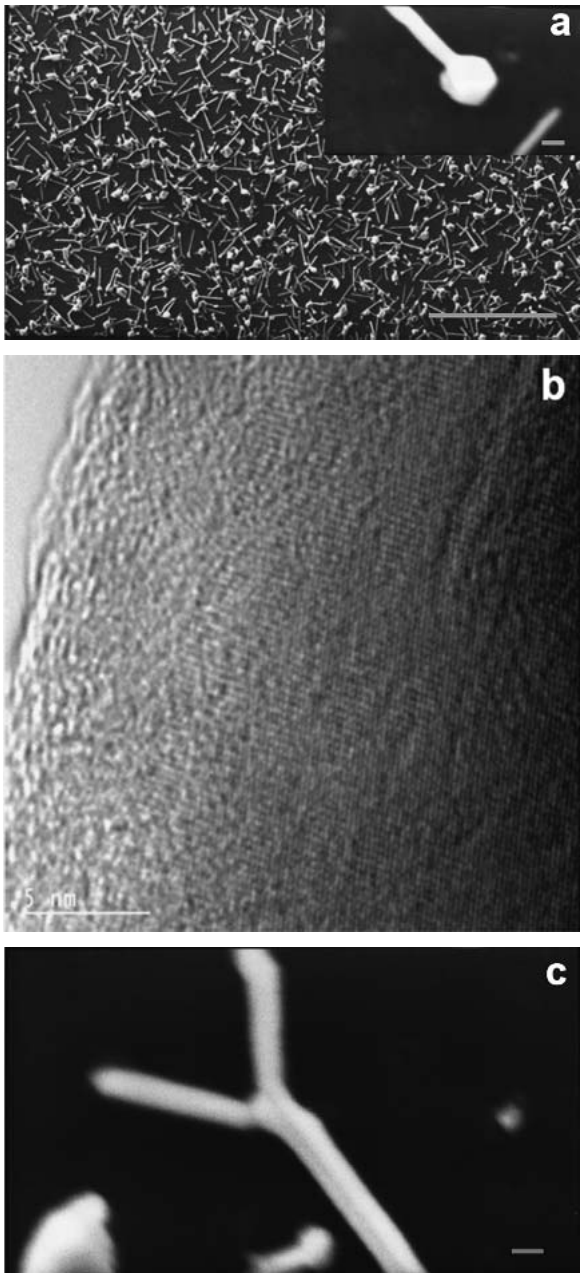

FIG. 5. (a) The SEM image of indium oxide nanorods (growth condition: Ar 200 sccm; 5–7 h; atmosphere pressure; 1000 °C). The scale bar corresponds to 10 μm. Inset: The scale bar is 100 nm. (b) The TEM image of an indium oxide nanorod. (c) SEM image of branched structure. The scale bar corresponds to 100 nm.

In principle, indium oxide is a very promising candidate for field emission because of its relatively low electron affinity (~3.5 eV), convenience of *n*-type doping (e.g., Sn-doped indium oxide), higher chemical inertness, and higher sputter resistivity. However, shaping the emitter of these materials is still challenging and cannot be achieved by the conventional chemical etching technique. Because the In_2O_3 pyramids described in this article possess extremely small radius of curvature at their tips, they are expected to exhibit stable and efficient field emission. Figure 6 illustrates the field-emission characteristics measured from nanopyramids. The turn-on electric field (defined as applied field required to obtain current density of 0.1 $\mu A/cm^2$) is estimated to be 2.7 V/μm. The emission-current density reached about 1 mA/cm^2, which can guarantee sufficient brightness in the flat panel display applications, at threshold field of about 6.0 V/μm. The current density J versus applied field E can be understood using the Fowler–Nordheim equation:[20]

$$J = A(\beta^2 E^2/\phi)\exp(-B\phi^{3/2}/\beta E) \quad ,$$

where ϕ is the work function, A and B are constants, β is field-enhancement factor that is associated with magnitude of the electric field at the emitting surface by E local $= \beta E$, and E local is local electric field at the emitting surface. The Fowler–Nordheim (F–N) plot ($\ln(J/E^2)$ vs. $1/E$) shows a linear relationship in the range below current saturation and confirms that the emitted current is indeed caused by vacuum tunneling (Fig. 6, inset). The value of current saturation, which is ascribed to depletion of free electrons in the conductive band, can easily be improved by *n*-doping method, such as, for example, Sn-doped indium oxide. The field-enhancement factor β for nanopyramids is about 1600, which is calculated from the slope of a straight section of the F–N plot. The performance of emission from the nanopyramids is striking and comparable with that of carbon nanotubes.[21] Moreover, it is easy to control the size and density of pyramids on substrate by tuning reaction parameters to enhance further the current density and uniformity of emission current. The tip-shaped emitters of the indium oxide will make the fabrication of the Spindt-type triode structure a more straightforward process because this technique has the advantage of low cost, easy growth position (owing to the selective deposition of the nickel catalyst), potential for scale-up production, and ability to integrate with silicon substrate.

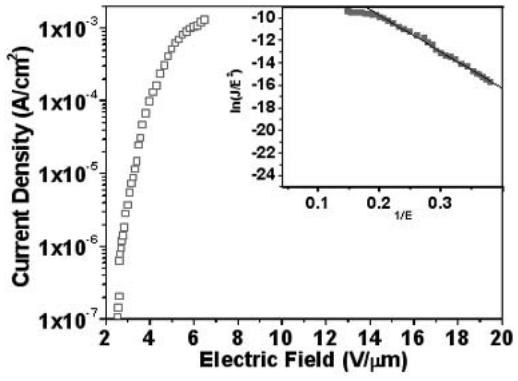

FIG. 6. The emission-current density from In_2O_3 pyramids (average size about 180 nm). The turn-on field, 2.7 V/μm; the threshold field, 6.0 V/μm; $\beta = 1600$. Inset: F–N plot.

IV. CONCLUSIONS

We have described the synthesis of cubic indium oxide micro- and nanopyramids on the silicon wafer via selective epitaxial VS growth through a methane-assist thermal reduction method. The size, morphology, and density of pyramids can easily be controlled by tuning reaction parameters. The method also has good compatibility with other procedures involved in conventional microfabrication processes. In_2O_3 pyramids are very promising for some vacuum microelectronic applications, such as, for example, the cold-cathode in flat panel displays. Laterally grown indium oxide nanorods on the silicon wafer were also prepared via a VLS mechanism. The laterally grown In_2O_3 nanorods take advantage of ideal configuration, facilitating their use in building high-sensitivity gas sensors for toxic NO_2 gas exhausted from automobiles.

ACKNOWLEDGMENTS

Dr. Ye Zhang and Mr. Hongbo Jia contributed equally to the work. This work was supported by the National Natural Science Foundation of China (Grant No. 50025206), the Research Fund for the Doctoral Program of Higher Education (RFDP) of China, and Jun-Zheng Fund of Peking University, China.

REFERENCES

1. I. Hamberg and C.G. Granqvist, J. Appl. Phys. **60,** R123 (1986).
2. A.G.U. Perera, H.C. Liu, and M.H. Francombe, *Semiconductor Optical and Electro-Optical Devices* (Academic Press, London, U.K., 2000).
3. H. Kim, A. Pique, J.S. Horwitz, H. Mattoussi, H. Murata, Z.H. Kafafi, and D.B. Chrisey, Appl. Phys. Lett. **74,** 3444 (1999).
4. H. Yumoto, S. Onozumi, Y. Katoh, M. Ishihara, and K. Kishi, Crystal Res. Technol. **31,** 159 (1996).
5. I. Hamberg and C.G. Granqvist, Appl. Phys. Lett. **44,** 721 (1984).
6. F. Stucki, P. Bruesch, and F. Greuter, Surf. Sci. **189,** 294 (1987).
7. M.S. Lee, W.C. Choi, E.K. Kim, C.K. Kim, and S.K. Min, Thin Solid Films **279,** 1 (1996).
8. E.J. Tarsa, J.H. English, and J.S. Speck, Appl. Phys. Lett. **62,** 2332 (1993).
9. J.C.C. Fan, F.J. Bachner, and G.H. Foley, Appl. Phys. Lett. **31,** 773 (1977).

10. M.J. Zheng, L.D. Zhang, X.Y. Zhang, J. Zhang, and G.H. Li, Chem. Phys. Lett. **334,** 298 (2001).
11. R.B.H. Tahar, T. Ban, Y. Ohya, and Y. Takahashi, J. Appl. Phys. **82,** 865 (1997).
12. L.A. Ryabova, V.S. Salun, and I.A. Serbinov, Thin Solid Films **92,** 327 (1982).
13. Z.W. Pan, Z.R. Dai, and Z.L. Wang, Science **291,** 1947 (2001); C.H. Liang, G.W. Meng, Y. Lei, F. Phillipp, and L.D. Zhang, Adv. Mater. **13,** 1330 (2001); H.J. Zhou, W.P. Cai, and L.D. Zhang, Appl. Phys. Lett. **75,** 495 (1999).
14. M.A. Green, J. Zhao, and A. Wang, *2nd World Conference and Exhibition on Photovoltaic Solar Energy Conversion*, Vienna, 1187 (1998).
15. Z.L. Wang, J. Phys. Chem. B **104,** 1153 (2000); Y.G. Sun and Y.N. Xia, Science **298,** 2176 (2002).
16. P. Campbell and M.A. Green, J. Appl. Phys. **62,** 243 (1987).
17. M. Chhowalla, K.B.K. Teo, C. Ducati, N.L. Rupesinghe, G.A.J. Amaratunga, A.C. Ferrari, D. Roy, J. Robertson, and W.I. Milne, J. Appl. Phys. **90,** 3508 (2001).
18. R.S. Wagner and W.C. Ellis, Appl. Phys. Lett. **4,** 89 (1964).
19. R.S. Wagner and C.J. Doherty, J. Electrochem. Soc. **115,** 93 (1968).
20. R.H. Fowler and L.W. Nordheim, Proc. R. Soc. (London) A **119,** 173 (1928).
21. W.A. de Heer, A. Châtelain, and D. Ugarte, Science **270,** 1179 (1995).